Magnetic dilution and steric effects in the multiferroic delafossite $CuCrO_2$

E. Pachoud,[1,*] K. Singh,[1] Y. Bréard,[1] C. Martin,[1] G. André,[2] V. Hardy,[1] Ch. Simon,[1] and A. Maignan[1]

[1]*Laboratoire CRISMAT, UMR 6508 CNRS, ENSICAEN, 6 bd du Maréchal Juin 14050 CAEN Cedex 4, France*

[2]*Laboratoire Léon Brillouin, UMR 12, CEA-Saclay, CEA-CNRS, 91191 GIF-SUR-YVETTE Cedex, France*

(Received 24 May 2012; published 21 August 2012)

In order to get to the bottom of substitution effects reported in $CuCrO_2$ delafossite, structural, magnetic, and electric properties of several $CuCr_{1-x}M_xO_2$ series, where M^{3+} is a $S = 0$ cation ($M^{3+} = Al^{3+}$, Ga^{3+}, Sc^{3+}, Rh^{3+}), have been investigated. It is shown that the homogeneity of the substitution is element dependent and is particularly difficult to achieve for the smallest Al^{3+} cation. Ferroelectricity and dielectric properties are found to depend on the x value, but also on the nature of M: The largest substitution effects are observed for the larger elements, owing to the decrease of the Cr^{3+}-Cr^{3+} interaction resulting from the enlargement of the in-plane lattice parameter. However, the magnetic structures of $CuCr_{0.9}Ga_{0.1}O_2$ and $CuCr_{0.9}Rh_{0.1}O_2$, revealed close to that of $CuCrO_2$ by neutron diffraction, demonstrate the great stability of this antiferromagnetic incommensurate structure against the presence of $\{M^{3+}, S = 0\}$ cations. This emphasizes the very different nature of the magnetic ground state of $CuCrO_2$, as compared to $CuFeO_2$, despite their common structural characteristics.

DOI: 10.1103/PhysRevB.86.054437 PACS number(s): 75.85.+t, 75.47.Lx, 61.05.fg, 77.80.−e

I. INTRODUCTION

Triangular lattice antiferromagnets are attracting much attention in the search for new spin induced ferroelectrics. This is illustrated by several examples, which belong to a same structural type containing CdI_2-type layers, that is, made of edge-shared MX_6 octahedra, where the M magnetic cations form a triangular network. Among them, one can quote the delafossites $CuCrO_2$[1] or the $CuFe_{1-x}M_xO_2$ series ($M^{3+} = Al^{3+}, Ga^{3+}, Rh^{3+}$),[2–4] and the derived sulfide $AgCrS_2$[5] for which only the crystallographic space group is polar. Indeed, more often magnetic frustration can lead to complex noncollinear magnetic structures in triangular lattices and some of them break the local inversion symmetry as the incommensurate screw magnetic structure of $CuCrO_2$.[6] In this type of two-dimensional (2D) compounds, the ratio between in- and out-of-plane magnetic exchanges, that is, in and between successive triangular layers, is playing a crucial role in the stabilization of such complex structures. Taking into account the importance of this exchange energy ratio and the tendency of the triangular network to become anisotropic to lift the degeneracy, it is to be expected that magnetic structures may be sensitive to subtle changes in chemical composition. This is illustrated by $CuFe_{1-x}M_xO_2$ ($M^{3+} = Al^{3+}$, Ga^{3+}, Rh^{3+} and $x \cong 0.01$–0.10) for which the collinear four sublattice of $CuFeO_2$ is changed into a ferroelectric incommensurate screw type magnetic phase.[7–12] In contrast, although the Mg^{2+} substitution for Cr^{3+} in $CuCrO_2$ drastically modifies the electronic conductivity,[13] the magnetic structure of $CuCr_{0.98}Mg_{0.02}O_2$ is similar to that of $CuCrO_2$.[6] However the effect of such an aliovalent substitution is difficult to study as 2% Mg substitution is found to be very close to the solubility limit,[14] calculated at 1.1% Mg in the $CuCr_{1-x}Mg_xO_2$ study.[15] The homogeneity of the substitution can also be a parameter to take into account for the results interpretation, even for isovalent substitutions. It is the case of the Al^{3+} for Cr^{3+} substitution in $CuCrO_2$ that is reported to induce a short-range magnetic behavior,[16] alike 2D antiferromagnetic excitations and interpreted as the appearance of a nontrivial state such as a spin-nematic or a spin-liquid state.[17] However the dielectric peak at T_N is still observed for $CuCr_{0.85}Al_{0.15}O_2$.[18] Nonetheless in Ref. 16, the Bragg peaks observed in the powder x-ray diffraction patterns are found to broaden with the increase of the Al^{3+} nominal content, a possible sign of chemical disorder. A similar observation has recently been made on $CuCr_{0.95}M_{0.05}O_2$ samples with M = Al, Sc, Rh, Co.[19] In the same way, the $CuCr_{1-x}Fe_xO_2$ series is not easily made, as structural disorder is evidenced by anisotropic broadening of peaks in the x-ray diffractograms.[20] Due to the Jahn-Teller distortion of Mn^{3+} ($t_{2g}{}^3e_g{}^1$), the manganese analog $CuMnO_2$ crystallizes in a monoclinic structure, the crednerite $C2/m$,[21] therefore complicating the formation of the solid solution $CuCr_{1-x}Mn_xO_2$. Although the $CuVO_2$ delafossite does not exists, V^{3+} ($3d^2$) can be incorporated in $CuCr_{1-x}V_xO_2$ up to $x = 0.5$,[22] and changes the antiferromagnetic ordering and the ferroelectricity of $CuCrO_2$ to spin glass and dipolar glass behaviors in $CuCr_{0.5}V_{0.5}O_2$.[23] Consequently, it appears that only a few elements can be considered to study the substitution effect on the B site.

Considering chemical substitutions in delafossite as a factor inducing or suppressing spin induced ferroelectricity, a complete investigation of the $CuCr_{1-x}M_xO_2$ series has been conducted, restricted to a $S = 0$ trivalent M element, which ability to lie at the Cr site of the delafossite is attested by the existence of the $CuMO_2$ compounds.[24–26] Particular attention was paid to low substitution levels, in analogy with the iron based delafossites. It is found that the magnetic properties depend on the size of the $3d$ cations [smaller (Al^{3+}), similar (Ga^{3+}), or larger (Sc^{3+}) than Cr^{3+}]. This result is compared to that obtained for Rh^{3+}, a $\{S = 0$–$4d$ ($t_{2g}{}^6e_g{}^0$)$\}$ cation whose orbitals are more extended than those of the $3d$ ones.

II. EXPERIMENT

The polycrystalline $CuCr_{1-x}M_xO_2$ samples (with $M^{3+} = Rh^{3+}$, Al^{3+}, Ga^{3+}, and Sc^{3+} and $x = 0.02, 0.05, 0.10$, and 0.15) were prepared by solid state reaction, starting from stoichiometric amounts of the corresponding precursor oxides (Cu_2O, Cr_2O_3, and M_2O_3). In addition, for $M^{3+} = Al^{3+}$, samples

were prepared for the whole solid solution. The mixtures were carefully ground and pressed in bars, which were heated at 1200 °C for 12 h in platinum (or alumina for $M^{3+} = Rh^{3+}$) crucibles in air. The quality of the samples was first checked by x-ray powder diffraction (XRD) at room temperature by using a Panalytical diffractometer equipped with a Cu$K\alpha$ source, in the 5° to 110° 2θ range. All the patterns present the peaks characteristic of the R-3m delafossite structure. Neutron powder diffraction (NPD) data were collected on the G4.1 instrument ($\lambda = 2.423$ Å), located at Orphée-LLB (CEA Saclay, France) for $CuCr_{0.9}Rh_{0.1}O_2$ and $CuCr_{0.9}Ga_{0.1}O_2$. They were set in thin-walled cylindrical vanadium cans, and the diffraction data were collected at chosen temperatures down to 1.8 K. Structural refinements were carried out on the XRD and NPD data using the Fullprof software.[27]

Transmission electron microscopy (TEM) was performed on selected samples ($CuCr_{0.9}Ga_{0.1}O_2$, $CuCr_{0.9}Sc_{0.1}O_2$, and $CuCr_{0.8}Al_{0.2}O_2$) by using a JEOL 2010 microscope operating at 200 kV, equipped with an energy dispersive spectroscopy (EDS) analyzer. The samples were carefully ground in an agate mortar in n-butanol, and one drop of this suspension was deposited on a nickel grid covered with a holey carbon film. Microstructural observations were also carried out with a Zeiss Supra 55 scanning electronic microscope (SEM) on small pieces of all the $CuCr_{0.9}M_{0.1}O_2$ samples.

Magnetic susceptibility (χ) vs temperature curves were recorded by using a Quantum Design SQUID magnetometer ($\chi = M/H$, where M and H are for the magnetization and the magnetic field, respectively). All the data were collected from 5 to 300 K in 0.3 T; zero field cooling (zfc) and field cooling (fc) processes were systematically used.

The measurements of electrical properties (ε', P) were performed in a Quantum Design 14T PPMS with a homemade measurement probe. The samples were shaped as thin plates about 0.50 mm thick and with a surface of 5 mm^2. Silver paste was used to make electrical contacts on the flat surfaces. Dielectric properties (ε') were measured at four frequencies (between 5 and 100 kHz) with 100 mV using an Agilent 4284A LCR meter. Data were collected during heating (2 K/min). Polarization (P) was measured using an automatic pyroelectric current integration by a Keithley 6517A electrometer. The samples were cooled in a poling electric field of 430 kV/m, which was then removed and the time dependence of polarization was recorded. The stabilization of the measurement was reached after a waiting time of about 5 ks, and then P vs T data were collected upon warming at 2 K/min.

III. RESULTS

As mentioned in the Introduction, since the properties can be very sensitive to the substitution, prior to the physical properties measurements, special care was taken to characterize the structures by combining powder x-ray diffraction and transmission electron microscopy. In the following, the structural characterizations are given first, the magnetic and electric properties are presented in a second section, and the results are then discussed in the third part.

A. Structural characterizations

The delafossite $CuCrO_2$ crystallizes at room temperature in the R-3m space group[28] [with $a = 2.9746(1)$ Å and $c = 17.1015(3)$ Å in the hexagonal setting]. The layered structure consists of a 1:1 stacking, along the c axis, of edge-shared CrO_6 octahedral sheets with layers of Cu^+ in dumbbell coordination. Both cations organize themselves in planar triangular networks [Fig. 1(a)]. Despite the fact that all the M cations in $CuCr_{1-x}M_xO_2$ are trivalent, different structural evolutions with x are observed depending on the nature of M.

(Rh) Despite the larger ionic radius of Rh^{3+} than Cr^{3+} ($r_{Rh^{3+}} = 0.665$ Å and $r_{Cr^{3+}} = 0.615$ Å[29]) the delafossite structure is preserved with the substitution. The structural refinements using x-ray diffractograms [Fig. 1(b)] lead to a monotonous increase of both unit cell parameters as x increases, in the $CuCr_{1-x}Rh_xO_2$ formula, up to $x = 0.15$ [for which $a = 2.9859(4)$ Å and $c = 17.1211(3)$ Å], in agreement with the solid solution already reported.[30]

(Ga) Even if the ionic radius of Cr^{3+} and Ga^{3+} are very close ($r_{Ga^{3+}} = 0.620$ Å) and if the delafossite $CuGaO_2$ exists, x-ray diffraction patterns show that tiny peaks characteristic of the $CuGa_2O_4$ spinel (Fd-3m SG, $a \sim 8.31$ Å[31]) are systematically observed in addition to those of the delafossite. This impurity is more easily detectable in SEM due to the

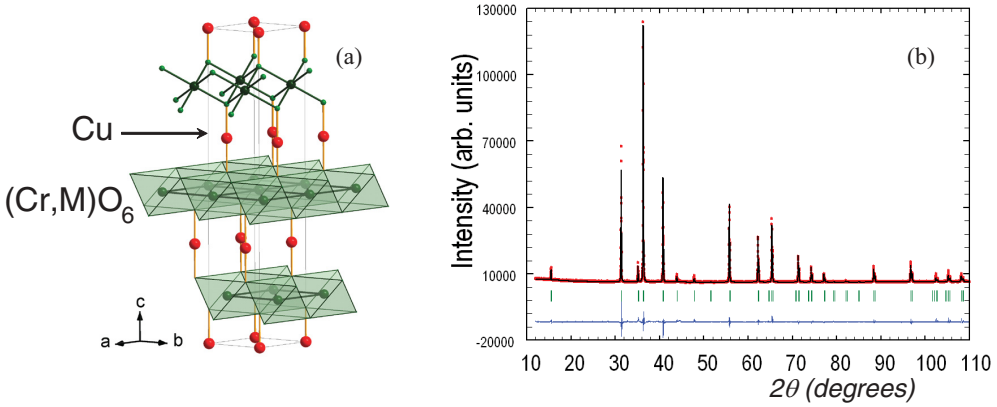

FIG. 1. (Color online) (a) Representation of the delafossite structure. (b) Experimental (red points), calculated (black line), and difference (bottom blue line) x-ray powder diffraction patterns of $CuCr_{0.9}Rh_{0.1}O_2$.

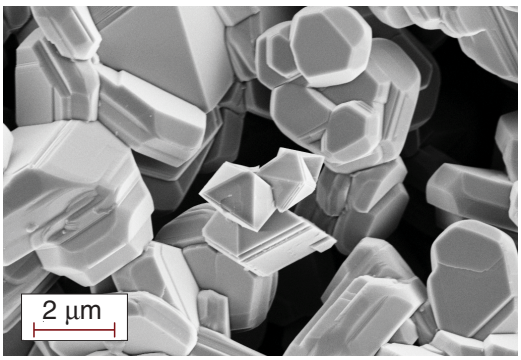

FIG. 2. (Color online) SEM image of $CuCr_{0.9}Ga_{0.1}O_2$ displaying octahedral crystals of the cubic spinel in a matrix of plateletlike microcrystals characteristic of the delafossite.

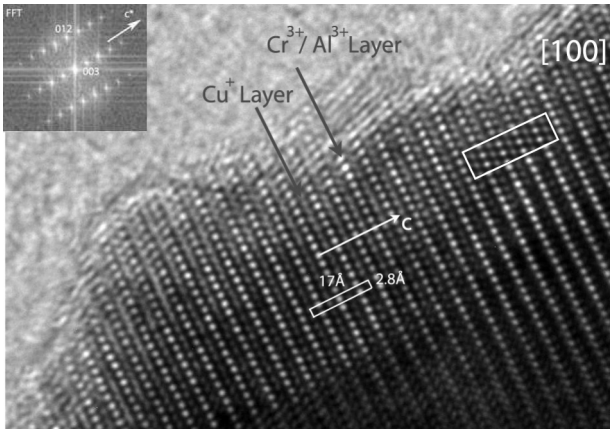

FIG. 4. HREM image of $CuCr_{0.8}Al_{0.2}O_2$ with the corresponding FFT on the top left and calculated image is inserted in the white rectangle.

octahedral shape of these small crystals, as displayed in Fig. 2. However, its amount does not exceed 1% in weight within the range $0 < x \leqslant 0.15$. Refinements using the XRD data lead to a slight increase of the a parameter with the substitution while c remains practically unchanged [$a = 2.9775(5)$ Å and $c = 17.1002(3)$ Å for $x = 0.15$]. The $CuCr_{0.9}Ga_{0.1}O_2$ sample has been characterized by TEM: Reconstruction of the reciprocal space confirms the space group R-3m at room temperature, and EDS analyses performed on about 20 microcrystals [selected by electron diffraction (ED) according to their rhombohedral structure] show that the distribution is homogeneous and close to the expected value $x = 0.10(3)$. The actual Ga for Cr substitution is also confirmed by the NPD results, as explained in the discussion.

(Al) In the case of the smallest substituting cation ($r_{Al^{3+}} = 0.535$ Å), the complete solid solution has been synthesized and all the samples exhibit XRD patterns characteristic of delafossite. Even if no impurities are detected for small x values by XRD and SEM, the structural refinements of the $CuCr_{1-x}Al_xO_2$ compounds reveal a nonmonotonous evolution of the lattice parameters with x [Fig. 3(a)]. According to the Al^{3+} radius and in agreement with the recently reported solid solution,[16] the values of the unit cell parameters (a and c) decrease with x, but a clear deviation from the Vegard's law is obtained for small aluminum contents ($x \leqslant 0.20$). A close inspection of the XRD patterns reveals tails for many Bragg peaks, a feature that is less pronounced for the (00l) reflections [Fig. 3(b)]. The $CuCr_{0.8}Al_{0.2}O_2$ sample was then carefully studied by TEM. The average composition obtained by EDS analysis is $x = 0.16$ with an important dispersion (from $x = 0.00$ to 0.30). The regular stacking along c of the delafossite structure is preserved within the crystallites as seen on the HREM [100] image in Fig. 4. The main structural difference between the limit compositions $CuCrO_2$ and $CuAlO_2$ lies in the variation of the a parameter, corresponding to a 4% decrease; whereas c remains almost unchanged (i.e., a variation <1%).[24] The observed shoulders (on the high angle side) in the lower part of the peaks in the x-ray diffractograms are thus explained by the inhomogeneous Al for Cr substitution, leading to a distribution of the cell parameters. It must also be pointed

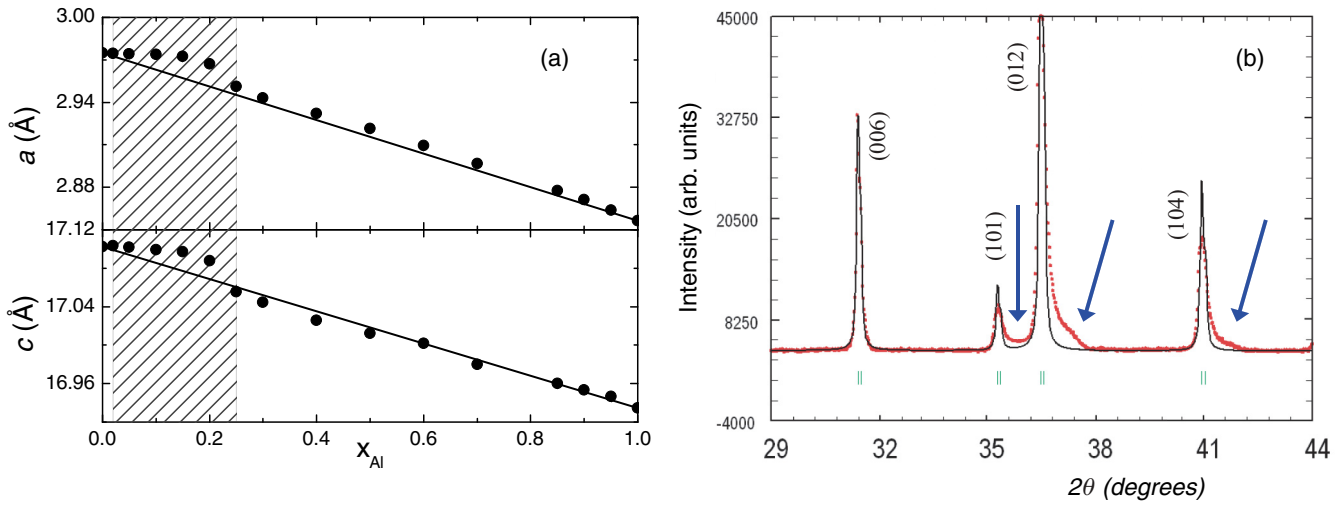

FIG. 3. (Color online) (a) Unit cell parameters of the $CuCr_{1-x}Al_xO_2$ series; the lines correspond to the Vegard's law, the hatched area correspond to the range in which Bragg peaks present tails as shown in (b). (b) Enlargement of the fitted x-ray diffractogram of $CuCr_{0.8}Al_{0.2}O_2$, arrows highlight the tails.

TABLE I. Characteristic parameters for $CuCr_{0.9}M_{0.1}O_2$.

M^{3+}	Al^{3+}	Cr^{3+}	Ga^{3+}	Rh^{3+}	Sc^{3+}
r (Å)	0.535	0.615	0.620	0.665	0.745
Electronic configuration	$2p^6$	$3d^3$	$3d^{10}$	$4d^6$	$3p^6$
a (Å)	2.97380(9)	2.97460(4)	2.97652(4)	2.98117(4)	2.99500(7)
c (Å)	17.0993(6)	17.1015(3)	17.0998(3)	17.1152(2)	17.0971(5)
V (Å^3)	130.958(7)	131.045(3)	131.201(3)	131.731(3)	132.814(6)
z_O	–	0.1069(3)	0.1084(2)	0.1055(2)	0.1075(3)
T_N (K)	24	25	24 17	16.5	–
θ_{CW} (K)	−200	−192	−160	−146	−123
χ_{5K} (emu/g)	4.38×10^{-5}	4.08×10^{-5}	2.77×10^{-5}	6.60×10^{-5}	3.09×10^{-5}
P_{5K} (μC/m^2)	9	24	–	18	–

out that no improvement in the Cr/Al distribution was achieved by changing the synthesis parameters such as reaction temperature, duration, atmosphere, etc.

(Sc) Despite the larger ionic radius of $r_{Sc}{}^{3+}$ (0.745 Å) compared with $r_{Cr}{}^{3+}$, single phase $CuCr_{1-x}Sc_xO_2$ samples are obtained from $x = 0$ to 0.15. Here again, the substitution mainly affects the a parameter, which increases up to 3.006(1) Å for $x = 0.15$ and c is kept almost unchanged at 17.0965(9) Å. This effect is thus slightly different from what is observed for Rh^{3+}, whose size is intermediate between Cr^{3+} and Sc^{3+}. The peaks of the XRD patterns become broader as the level of substitution increases and again the effect is less pronounced for the $(00l)$ reflections (not shown). The ED study on $CuCr_{0.9}Sc_{0.1}O_2$ reveals that some microcrystals present diffuse rings, but EDS analyses on about 20 well-crystallized microcrystals show a good homogeneity of the Sc content from one crystallite to another, $x = 0.09(2)$. Increasing the reaction temperature, in order to improve the sample quality, results in the rapid formation of impurities [like Cu_4O_3 and $(Cr,Sc)_2O_3$].

To summarize this structural part, our results show that the evolutions of the unit cell parameters are in agreement with the ionic radius of the substituting cations [$r_{Al}{}^{3+} < (r_{Ga}{}^{3+} \approx r_{Cr}{}^{3+}) < r_{Rh}{}^{3+} < r_{Sc}{}^{3+}$]. The effect of the substitution is more visible in the variation of the a parameter, as shown for all the $CuCr_{0.9}M_{0.1}O_2$ compounds (Table I). It is clear that the homogeneity range of the substitutions at the Cr site in $CuCrO_2$ strongly depends on M, and that synthesis difficulties are encountered in the large x range just using conventional solid state "shake and bake" method. For each series it is thus necessary to balance the analysis of the physical properties with the results of the structural study. This difficulty in the preparation of samples could be at the origin of the discrepancies observed in the literature about the properties of these materials.

B. Physical properties

1. Magnetism

(a) $r_M{}^{3+} > r_{Cr}{}^{3+}$. For these larger cations, in addition to the dilution effect, substitutions also modify the lattice parameters, and particularly the increase of the a parameter, that is, of the Cr^{3+}-Cr^{3+} distance in the (ab) plane, may weaken the magnetic exchanges. In that respect, the case of rhodium is even more complex: As not only the a parameter increases but the different hybridization of the $4d$ orbitals might play also a role on the properties.

(Rh) The $\chi(T)$ curve of $CuCrO_2$ is characterized by the existence of a magnetic transition at $T_N \cong 25$ K,[32] on which the Rh^{3+} for Cr^{3+} substitution has a dramatic effect. While T_N decreases with increasing level of substitution, down to $T_N = 11.5$ K for $x = 0.15$, the transition becomes sharper, in connection with larger χ values [Fig. 5(a)]. This evolution of the magnetic transition might reflect a more pronounced three-dimensional (3D) character of the magnetic structure. This kind of shape is similar to what has been observed in the Mg^{2+} substituted $CuCrO_2$, but in this case, the transition temperature as well as the magnetic structure were kept unchanged.[6]

The θ_{CW} obtained from the Curie-Weiss law fit in the paramagnetic state (above 200 K) increases with the substitution. This temperature is close to −192 K for the pristine compound, and reaches −122 K for $x = 0.15$, which could be a sign of a weakening of the antiferromagnetic interactions. The Néel temperature T_N also decreases with x, but more slowly than $|\theta_{CW}|$.

(Sc) As for Rh, the Néel temperature decreases as x increases in the $CuCr_{1-x}Sc_xO_2$ series, this trend being even more pronounced as $T_N \approx 13$ K for $x = 0.05$ against $T_N \approx 20$ K for $CuCr_{0.95}Rh_{0.05}O_2$. However, the shape of the anomaly in the $\chi(T)$ curves is different: As soon as $x = 0.05$, the downward transition below T_N of $CuCrO_2$ is replaced by an upturn [Fig. 5(b)]. Such an evolution for the $\chi(T)$ curves for the largest amounts of substitution is in marked contrast with the results of the $CuCr_{1-x}Al_xO_2$ series, those description follows.

(b) $r_M{}^{3+} < r_{Cr}{}^{3+}$: (Al). As explained in the structural section, for aluminum the very small decrease of the unit cell parameters has to be taken with caution as the extracted values correspond to the main peaks in the diffractograms, that is, to an actual x value smaller than the nominal one. However, our results [Fig. 5(c)] are similar to those previously reported in Ref. 17: There is a progressive disappearance of the magnetic transition. Nevertheless in our case, even if the transition is broader before vanishing, there is no indication of an additional lower T_N as in Ref. 17. The magnetic transition temperature is kept unchanged at $T_N \cong 25$ K in the $0 \leqslant x \leqslant 0.20$ range, in agreement with the inhomogeneous character of the substitution discussed in the first section. Furthermore, this transition on the $\chi(T)$ curves is suppressed for larger x values. For $T > T_N$, contrasting with the substitutions by Rh^{3+}

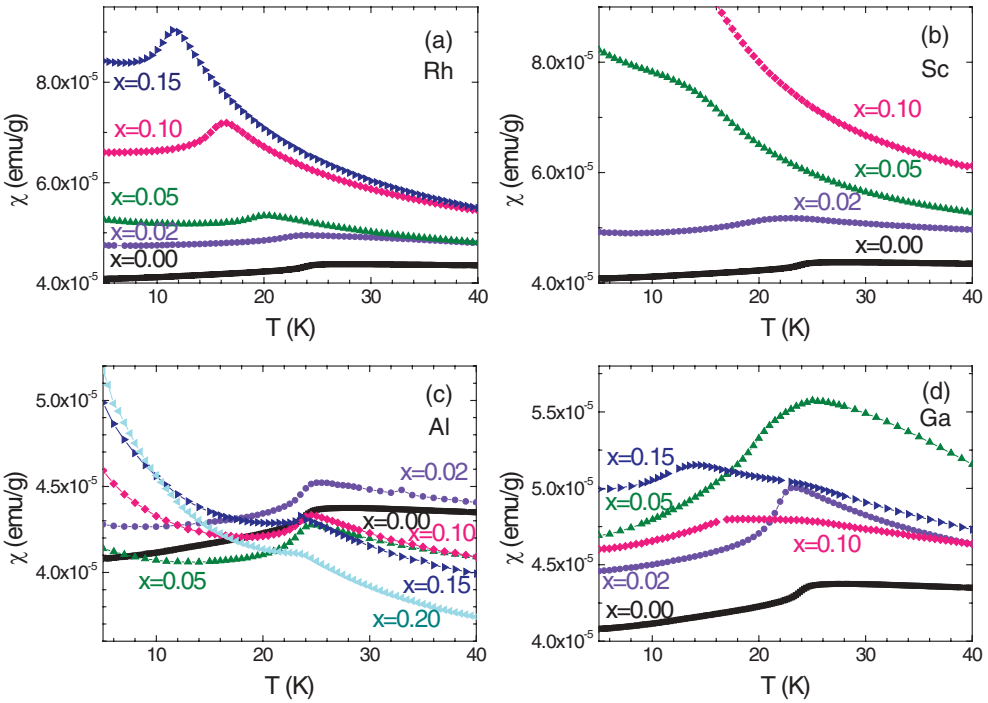

FIG. 5. (Color online) zfc magnetic susceptibilities as a function of temperature of $CuCr_{1-x}M_xO_2$ (in 0.3 T) with M = Rh (a), Sc (b), Al (c), and Ga (d).

or Sc^{3+}, the $\chi(T)$ values appear to be systematically shifted down as the Al^{3+} content increases and concomitantly, below T_N, a paramagnetic Curie tail is induced.

(*c*) ${r_M}^{3+} \approx {r_{Cr}}^{3+}$: (Ga). This $CuCr_{1-x}Ga_xO_2$ series allows studying an effect of magnetic dilution without steric effect since the unit cell parameters are almost unchanged, as shown in the previous section. This particularity among the four series is confirmed by the magnetic measurements: The impact of the Ga substitution on the $\chi(T)$ curves [Fig. 5(d)] differs from those of all other cations, as shown for the $x = 0.10$ series in Fig. 6. First, for the $x = 0.02$ and $x = 0.05$ compositions, the χ values increase with x and the transition at $T_N \cong 25$ K is more pronounced. Second, for larger x values ($x = 0.10$ and $x = 0.15$, see also inset of Fig. 6), two changes of slope are detected, which suggest the existence of two characteristic temperatures,

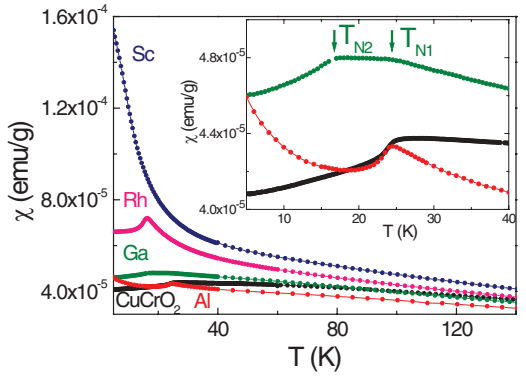

FIG. 6. (Color online) zfc $\chi(T)$ curves for $CuCr_{0.9}M_{0.1}O_2$ (in 0.3 T), M cations are labeled in the graph. The inset corresponds to the enlargement of the left down area of the main panel.

the first one at ≅25 K as for $CuCrO_2$,[32] and the second one at a lower temperature, decreasing from ≅17 to ≅14 K for $x = 0.10$ and $x = 0.15$, respectively. These curves are reminiscent of the delafossite $CuFeO_2$, which undergoes two successive magnetic transitions at $T_{N1} = 14$ K from paramagnetic to an incommensurate structure, which becomes commensurate at $T_{N2} = 11$ K.[33,34]

2. *Electrical properties*

(a) Dielectric permittivity. The multiferroic $CuCrO_2$ and $AgCrO_2$ ceramics were previously shown to exhibit a dielectric peak at T_N,[1] which reflects the setting of the antiferromagnetism. This was taken as evidence for magnetodielectric coupling and motivated the measurements of the dielectric permittivity as a function of temperature for the $CuCr_{1-x}M_xO_2$ series.

(Rh) In the $0 \leqslant x \leqslant 0.10$ range, a dielectric peak is observed at a temperature which decreases as x increases [Fig. 7(a)]. The dielectric losses are very low ($<10^{-2}$), and also present an anomaly at the same temperature (not shown). This evolution with x reflects the decrease of the antiferromagnetic transition temperature in the $\chi(T)$ curves [Fig. 5(a)], which illustrates the coupling between the magnetic and dielectric properties in these delafossites.

(Sc) Similarly to the $\chi(T)$ curves where the magnetic transition disappears rapidly with x [Fig. 5(b)], the transition on the $\varepsilon'(T)$ curve remains visible only up to $x = 0.02$ (not shown). This confirms the strong impact of the Sc^{3+} substitution that hinders magnetic ordering.

(Al) The effect is more progressive in this case. The substitution induces a broadening of the dielectric peak [Fig. 7(b)], with a decrease of the relative magnitude as the

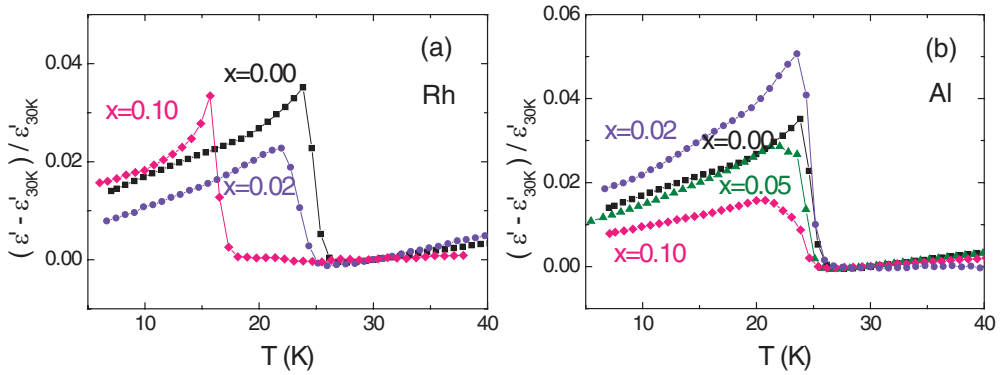

FIG. 7. (Color online) Normalized dielectric permittivity as a function of temperature of $CuCr_{1-x}M_xO_2$ (100 kHz) with M = Rh (a) and Al (b).

Al^{3+} content increases. In contrast to Rh^{3+} and Sc^{3+}, the characteristic transition temperature on the $\varepsilon'(T)$ curve is kept unchanged with x, reflecting the unchanged T_N observed on the magnetic susceptibility curves [Fig. 5(c)].

(Ga) For this cation also, the changes in the $\chi(T)$ curves are in agreement with anomalies in the $\varepsilon'(T)$ curves. Accordingly, when two magnetic transitions are present in the $\chi(T)$ curve, as for the $x = 0.10$ and $x = 0.15$ compounds, two accidents are also detected in the $\varepsilon'(T)$ curve (Fig. 8).

(b) Electric polarization. The results of the magnetic and dielectric measurements emphasize the different behavior of the Al-substituted samples. For Rh, Sc, and Ga, at least one characteristic temperature decreases as the content of foreign element increases, whereas in the Al case, T_N is kept unchanged. This could be explained by the chemical inhomogeneity observed in this series, the existence of regions where the Al^{3+} content is much smaller ($\rightarrow 0$) than the nominal one could explain the persistence of a magnetic transition around 25 K. Referring to $CuCrO_2$ for which ferroelectricity is induced by the setting of the noncollinear antiferromagnetic structure, electric polarization measurements were performed for Rh- and Al-substituted samples.

For the $CuCr_{1-x}Rh_xO_2$ series [Fig. 9(a)], the $P(T)$ curves corresponding to $x = 0.02$ and $x = 0.10$ show that the ferroelectric Curie temperature (T_C) follows the evolution of T_N with x. Only a slight decrease of the P value at 6 K, from 24 $\mu C/m^2$ for $CuCrO_2$ down to 18 $\mu C/m^2$ for $x = 0.10$, is observed, and no polarization could be measured for $x > 0.10$. This result emphasizes that this substituted delafossite remains a multiferroic until dilution becomes too detrimental to the magnetic ordering. The coincidence between T_N, T_C, and the ε' peak temperature confirms the spin induced ferroelectricity. Also, the decrease of these three temperatures with x reflects the homogeneous distribution of Rh on the Cr sites.

In contrast, for the $CuCr_{1-x}Al_xO_2$ series [Fig. 9(b)], the $P(T)$ curves reveal unchanged T_C values as x increases up to $x = 0.10$, value beyond which P becomes no longer measurable. The three coinciding temperatures, T_N, T_C, and that of the ε' peak, are not changing with x, but the P value decreases with x. It is thus reasonable to ascribe the polarization origin to the presence of almost nonsubstituted regions (with compositions near $CuCrO_2$ and whose amount decreases with increasing x).

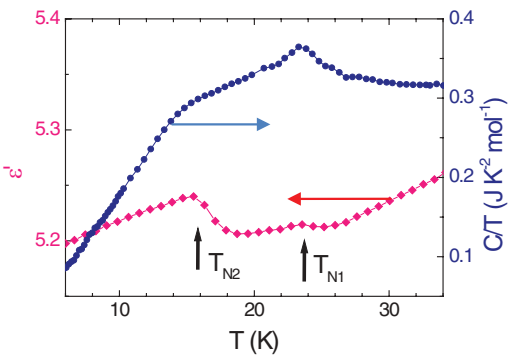

FIG. 8. (Color online) Evolution with temperature of the dielectric permittivity (100 kHz) (left axis) and of the specific heat C/T (right axis) of $CuCr_{0.9}Ga_{0.1}O_2$.

IV. DISCUSSION

In the $CuCrO_2$ system, the Cr substitution by small amount of different $\{S = 0, 3d, \text{or } 4d\}$ nonmagnetic trivalent cations induces various effects on the properties. Structurally, all the compounds crystallize in the delafossite space group $R\text{-}3m$, and the substitution mainly affects the a parameter, which follows the size of the cation at a fixed substitution level. As this unit cell parameter corresponds to the Cr^{3+}-Cr^{3+} distance, the change in a affects the magnetic coupling, as shown by the characteristic parameters (magnetic susceptibility curves) summarized in Table I (in Fig. 6) for the four $x = 0.1$ compounds. This is also illustrated in Fig. 10 where the Curie-Weiss temperature is plotted as a function of x for the four investigated series. The Curie-Weiss law is obeyed for all the compounds at sufficiently high temperature ($T \geqslant 200$ K) leading systematically to effective moment values (μ_{eff}) of $\cong 3.8$ μ_B per Cr, thus close to the expected value of 3.87 μ_B for Cr^{3+}. For Rh^{3+} and Sc^{3+} (larger than Cr^{3+}), θ_{CW} increases with x, revealing the weakening of the magnetic interactions as the Cr^{3+}-Cr^{3+} distance increases. According to the similar radius of Ga^{3+} and Cr^{3+}, θ_{CW} only increases up to -160 K for $x_{Ga^{3+}} = 0.10$, to be compared to -123 K for $x_{Sc^{3+}} = 0.10$. Thus, the θ_{CW} change in the Ga case corresponds to a pure dilution effect, whereas Sc has in

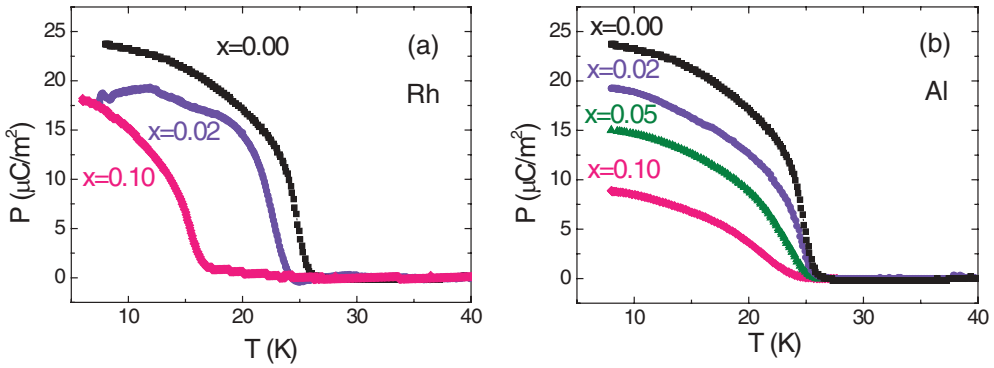

FIG. 9. (Color online) Variation of the polarization with temperature in $CuCr_{1-x}M_xO_2$ (after cooling with an applied electric field of 430 kV/m) for M = Rh (a) and Al (b).

addition a steric effect. The Al case has to be discussed more cautiously. As shown in Fig. 10, the θ_{CW} decrease agrees with the shortening of the Cr^{3+}-Cr^{3+} distance which could compensate the magnetic dilution effect. Nonetheless, a nonhomogeneous Al distribution in the matrix is evidenced, supported by the $\chi(T)$ curves which indicate that the magnetic ordering temperature remains unchanged with x. This confirms the previous report on $CuCr_{1-x}Al_xO_2$ ($x \leqslant 0.20$) by Okuda *et al.*[17] Although only one transition is visible in our magnetic susceptibility curves, a similar progressive disappearance of the transition without T_N evolution is observed, pointing out the inhomogeneous distribution of aluminum in the chromium matrix as well. Both studies confirm the difficulty of the formation of the $CuCr_{1-x}Al_xO_2$ solid solution.

As a consequence of both magnetic dilution and steric effects, the changes in the θ_{CW} values can be related to those in T_N. For the larger cation Sc^{3+}, the increase of the Cr^{3+}-Cr^{3+} distance is detrimental to the magnetic ordering with a rapid T_N decrease as the substitution amount increases (Fig. 10).

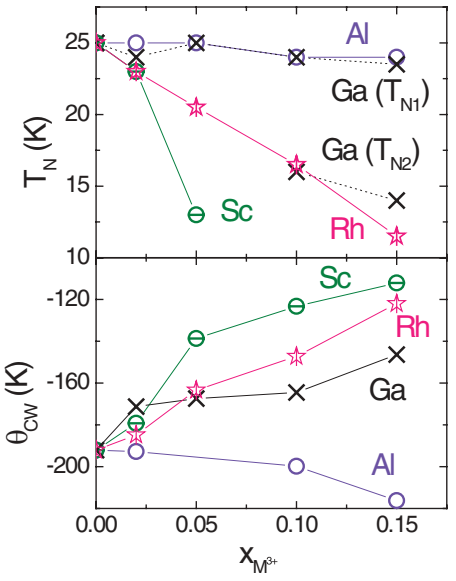

FIG. 10. (Color online) Variation of the characteristic magnetic temperatures T_N (upper part) and θ_{CW} (lower part) with the level of substitution for the four series.

The interesting effects on T_N and θ_{CW} induced in the Rh and Ga series motivated a neutron powder diffraction test to shed light on the magnetic structure of both compounds. Low-temperature NPD data were recorded on G4.1 for $CuCr_{0.9}Ga_{0.1}O_2$ (Fig. 11) and $CuCr_{0.9}Rh_{0.1}O_2$ (Fig. 12) to be compared to the known magnetic structure of $CuCrO_2$.

For $CuCr_{0.9}Ga_{0.1}O_2$, the delafossite structure R-3m is preserved from 300 down to 1.8 K, as for $CuCrO_2$.[6] Taking advantage of the difference between the scattering lengths of Cr and Ga for neutron diffraction, b_{Ga} (0.7288×10^{-12} cm) $\cong$ $2 \times b_{Cr}$ (0.3635×10^{-12} cm), the analysis of the NPD data allows to confirm the 0.9:0.1 Cr/Ga ratio [refined value: $x_{Ga} = 0.10(1)$]. The magnetic peaks observed at 1.8 K correspond to a propagation vector (q q 0) with $q \sim 0.329$ and are significantly broadened compared to the crystal structure peaks, which is a sign of magnetic disorder. This indicates that the magnetic structure observed in $CuCrO_2$ is not modified by substitution—in the limit of the experimental resolution—a result in strong contrast with the effect of such a substitution

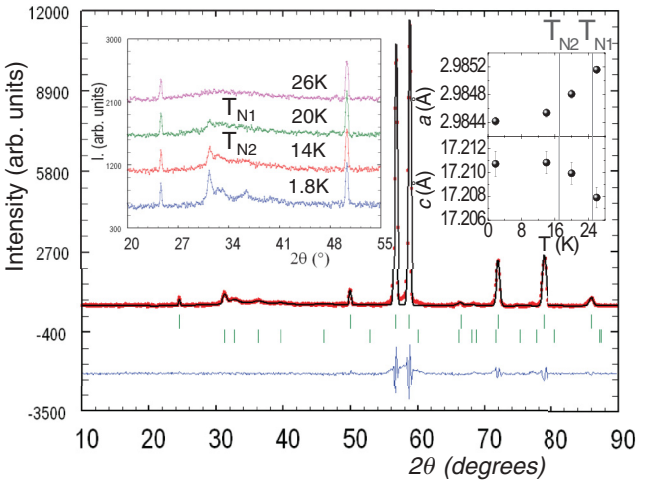

FIG. 11. (Color online) Refined NPD pattern ($\lambda = 2.428$ Å) of $CuCr_{0.9}Ga_{0.1}O_2$ (red dots, black lines, and blue lines are for experimental, calculated, and difference, respectively). The two sets of reflection markers indicate the nuclear (delafossite R-3m) and magnetic [helicoidal (q q 0) $q \sim 0.329$] structures. Insets: Low angle part of the NPD patterns recorded at four temperatures (left) and corresponding lattice parameters vs T (right).

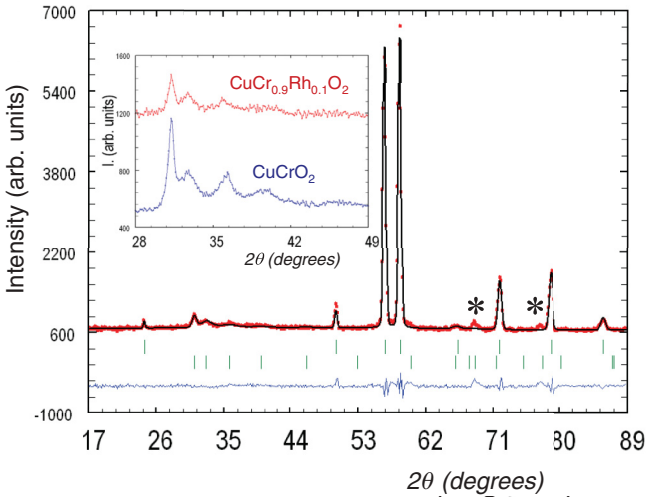

FIG. 12. (Color online) Refinement of the 2 K neutron powder diffractograms of $CuCr_{0.9}Rh_{0.1}O_2$. The upper (lower) row of vertical ticks indicates for the crystalline (magnetic) Bragg reflections. The stars correspond to reflections due to the instrumental setup. In the inset is shown the comparison between the low temperature $CuCrO_2$ (blue) and $CuCr_{0.9}Rh_{0.1}O_2$ (red) NPD data.

in $CuFeO_2$, but similar to the effect of Mg substitution in $CuCrO_2$. Further investigation was performed recording a NPD diagram at 20 K, that is, in the $\chi(T)$ plateau between T_{N1} and T_{N2} (inset of Fig. 6). No specifically different features can be identified at this temperature (inset of Fig. 11), at which the magnetic orders starts to set in, with the appearance of the first antiferromagnetic Bragg peak. At 26 K, just above T_{N1}, short-range magnetic interactions remain in the form of a broad magnetic diffuse scattering (around 32°). Even if these data do not allow a complete analysis of the magnetic order, they show unambiguously that the magnetic structure of $CuCrO_2$ is not very sensitive to this substitution. Despite this lack of a clear change in the magnetic structure between both T_N, the existence of two magnetic transitions in the T-dependent magnetic susceptibility of $CuCr_{0.9}Ga_{0.1}O_2$ is confirmed by specific heat measurements. The $C_p(T)$ curve exhibits a transition at $\cong$24 K, and a crossover around 15 K is clearly visible on the $C/T(T)$ curve (Fig. 8) which is related to the change of the slope about 17 K on the $\chi(T)$ curve. This second contribution is not observed for polycrystalline $CuCrO_2$, for which only one anomaly is visible at 25 K.[1,6,13,32] However, the number of magnetic transition in $CuCrO_2$ has recently become a controversial subject. Kimura *et al.* have observed two transition temperatures for out-of-plane and in-plane magnetic susceptibility measurements on single crystals, respectively, $T_{N2} = 24.2$ K and $T_{N1} = 23.6$ K, and polarization appears below T_{N1}.[35] A single crystal neutron diffraction study proposed to attribute these two temperatures to a two step process: The magnetic structure is a two-dimensional helicoid between T_{N2} and T_{N1}, and became three dimensional through ferromagnetic interlayer exchange below T_{N1}[36] but it does not allow the lack of ferroelectricity between both temperatures to be explained. On the other hand, a thorough single crystal study reveals a not so large difference between in-plane and out-of-plane magnetic measurements, with an unique transition temperature, corroborated by specific heat measurement.[37] In contrast to these inconsistencies, whose origin could be linked to the different methods used in the preparation of the single crystals, the observation of two magnetic transitions in $CuCr_{1-x}Al_xO_2$ was interpreted without any doubt as corresponding to inhomogeneous compounds (i.e., residual $CuCrO_2$ in an Al-substituted matrix in which the magnetic interactions between the chromium layers are reduced).[17]

The corresponding T_{N1} and T_{N2} values for $CuCr_{1-x}Ga_xO_2$ are reported on the $T_N = f(x)$ of Fig. 10. The origin of the second transition remains to be elucidated, by collecting neutron diffraction data at more temperatures and with longer acquiring time to track subtle evolution in the magnetic structure, and x-ray synchrotron diffraction to look for structural transition, or by measuring magnetic susceptibility on single crystals to check for an anisotropic magnetic behavior. Indeed $CuCr_{0.9}Ga_{0.1}O_2$ deserves further studies to understand the behavior below T_{N2}, even from a structural point of view, to follow more precisely the negative thermal expansion of the c parameter (inset of Fig. 11). In fact such studies could be a way to clarify how the ordered magnetic state sets up in the $CuCrO_2$ parent compound.

The lack of strong substitution effect on the magnetic structure of $CuCrO_2$ is confirmed by the NPD study of $CuCr_{0.9}Rh_{0.1}O_2$ (Fig. 12) and thus contrasts with the effects reported for $CuFeO_2$[7–12] for which the substitutions by Al^{3+}, Ga^{3+}, or Rh^{3+} induce a ferroelectric state, concurrently with a T_{N2} decrease. Consequently, the significant differences in the magnetic structures of $CuCrO_2$ and $CuFeO_2$ are probably at the origin of differences in the substitution effects. Whereas in $CuFeO_2$ the 3D collinear commensurate structure is well established, the weak intensities of the magnetic peaks (and their broadening) observed in polycrystalline $CuCrO_2$ reveal a more 2D structure, that is, disordered along the c axis. This singularity has been explained by different exchange energy ratio between in- and out-of-plane magnetic interactions. Indeed, inelastic neutron scattering performed on $CuCrO_2$ reveals the predominance of the in-plane interactions vs the weak out-of-plane magnetic ones and the role of the latter upon the incommensurability of the magnetic structure.[38,39] In contrast, the difference of strength between all the magnetic interactions is smaller in the ground state of $CuFeO_2$.[40] The Ga for Fe substitution, which alters the well ordered four sublattice collinear structure into an incommensurate helicoidal antiferromagnetic phase, mainly weakens the out-of-plane interactions.[41] The dilution effect seems to follow the same trend in substituted $CuCrO_2$, that is, affecting mainly the interactions along the c axis. Indeed, elastic neutron scattering experiment performed on $Cu_{1-x}Ag_xCrO_2$ and $CuCr_{1-x}Al_xO_2$ reveal an accentuated 2D character of the magnetic structure for both compounds.[13,17] However, as the structure of $CuCrO_2$ may be already considered as disordered (with weak out-of-plane interactions), substitution has a minor effect, as attested by the closeness of the NPD patterns of $CuCrO_2$,[6] $CuCr_{0.98}Mg_{0.02}O_2$,[6] $CuCr_{0.9}Ga_{0.1}O_2$ (Fig. 11), or $CuCr_{0.9}Rh_{0.1}O_2$ (Fig. 12). Thus, substitutions on chromium or iron magnetic networks have distinct effects because of the different magnetic ground states. In the same way, a different impact on the ferroelectricity can be anticipated in Cr and

Fe-based delafossites. Substitutions bring ferroelectricity in $CuFeO_2$ by inducing an incommensurate antiferromagnetic structure. In $CuCrO_2$, corresponding substitutions leave the type of magnetic structure responsible for the spin induced ferroelectricity unchanged: The magnetic dilution will decrease T_N, and consequently T_C, as it is evidenced experimentally in $CuCr_{0.9}Rh_{0.1}O_2$ by observation of polarization [Fig. 9(a)].

The aim of this last part of the work was to check the impact of the substitutions upon the magnetic structure in $CuCrO_2$: It is clear that they do not differ strongly, that is, the same helicoidal incommensurate magnetic model may be used with a propagation vector (q q 0) with q close to 1/3; whatever changes induced in the physical properties. Nevertheless complementary investigations are necessary to go further in the discussion, to follow carefully the establishment of the magnetic order, and to determine if the incommensurability (q) is affected by the substitution (depending on x and M). Moreover we may expect that different signatures could be observed by inelastic neutron scattering.

V. CONCLUSION

In $CuCr_{1-x}M_xO_2$ with M = Rh, Sc or Ga, steric effects and magnetic dilution interact together to weaken the magnetic exchanges, but without changing drastically the antiferromagnetic structure. It shows that this helicoidal and incommensurate structure is highly adaptable and allows modifications of macroscopic magnetic behaviors and ferroelectric properties.

ACKNOWLEDGMENTS

The authors thank F. Damay (LLB, Saclay) for helpful discussions about magnetic structures. This work was supported by funding from French *Agence Nationale de la Recherche* (ANR-08-BLAN-0005-01).

*elise.pachoud@ensicaen.fr

[1] S. Seki, Y. Onose, and Y. Tokura, Phys. Rev. Lett. **101**, 067204 (2008).
[2] N. Terada, S. Mitsuda, T. Fujii, K. Soejima, I. Doi, H. A. Katori, and Y. Noda, J. Phys. Soc. Jpn. **74**, 2604 (2005).
[3] N. Terada, T. Nakajima, S. Mitsuda, H. Kitazawa, K. Kaneko, and N. Metoki, Phys. Rev. B **78**, 014101 (2008).
[4] E. Pachoud, C. Martin, B. Kundys, Ch. Simon, and A. Maignan, J. Solid State Chem. **183**, 344 (2010).
[5] K. Singh, A. Maignan, C. Martin, and Ch. Simon, Chem. Mater. **21**, 5007 (2009).
[6] M. Poienar, F. Damay, C. Martin, V. Hardy, A. Maignan, and G. André, Phys. Rev. B **79**, 014412 (2009).
[7] N. Terada, S. Mitsuda, K. Prokes, O. Suzuki, H. Kitazawa, and H. A. Katori, Phys. Rev. B **70**, 174412 (2004).
[8] T. Nakajima, S. Mitsuda, S. Kanetsuki, K. Prokes, A. Podlesnyak, H. Kimura, and Y. Noda, J. Phys. Soc. Jpn. **76**, 043709 (2007).
[9] S. Kanetsuki, S. Mitsuda, T. Nakajima, D. Anazawa, H. A. Katori, and K. Prokes, J. Phys.: Condens. Matter **19**, 145244 (2007).
[10] S. Seki, Y. Yamasaki, Y. Shiomi, S. Iguchi, Y. Onose, and Y. Tokura, Phys. Rev. B **75**, 100403(R) (2007).
[11] N. Terada, T. Nakajima, S. Mitsuda, H. Kitazawa, K. Kaneko, and N. Metoki, Phys. Rev. B **78**, 014101 (2008).
[12] N. Terada, T. Nakajima, S. Mitsuda, and H. Kitazawa, J. Phys.: Conf. Ser. **145**, 012071 (2009).
[13] T. Okuda, T. Kishimoto, K. Uto, T. Hokazono, Y. Onose, Y. Tokura, R. Kajimoto, and M. Matsuda, J. Phys. Soc. Jpn. **78**, 013604 (2009).
[14] A. Maignan, C. Martin, R. Frésard, V. Eyert, E. Guilmeau, S. Hébert, M. Poienar, and D. Pelloquin, Solid State Commun. **149**, 962 (2009).
[15] E. Guilmeau, M. Poienar, S. Kremer, S. Marinel, S. Hébert, R. Frésard, and A. Maignan, Solid State Commun. **151**, 1798 (2011).
[16] P. T. Barton, R. Seshadri, A. Knöller, and M. J. Rosseinsky, J. Phys.: Condens. Matter **24**, 016002 (2012).
[17] T. Okuda, K. Uto, S. Seki, Y. Onose, Y. Tokura, R. Kajimoto, and M. Matsuda, J. Phys. Soc. Jpn. **80**, 014711 (2011).
[18] M. Amami, C. V. Colin, P. Strobel, and A. B. Salah, Phys. B **406**, 2182 (2011).
[19] F. Jlaiel, M. Amani, N. Boudjada, P. Strobel, and A. B. Salah, J. Alloys Compd. **509**, 7784 (2011).
[20] M. Lalanne, A. Barnabé, F. Mathieu, and Ph. Tailhades, Inorg. Chem. **48**, 6065 (2009).
[21] J.-P. Doumerc, M. Trari, J. Töpfer, L. Fournès, J.-C. Grenier, M. Pouchard, and P. Hagenmuller, Eur. J. Solid State Inorg. Chem. **31**, 705 (1994).
[22] K. El Ataoui, J.-P. Doumerc, A. Ammar, J.-C. Grenier, L. Fournès, A. Wattiaux, and M. Pouchard, Solid State Sci. **7**, 710 (2005).
[23] K. Singh, A. Maignan, Ch. Simon, S. Kumar, C. Martin, O. Lebedev, S. Turner,and G. Van Tendeloo, J. Phys.: Condens. Matter **24**, 226002 (2012).
[24] J. P. Doumerc, A. Ammar, A. Wichainchai, M. Pouchard, and P. Hagenmuller, J. Phys. Chem. Solids **48**, 37 (1987).
[25] B. U. Köhler and M. Jansen, Z. Anorg. Allg. Chem. **543**, 73 (1986).
[26] E. F. Bertaut and J. Dulac, J. Phys. Chem. Solids **21**, 118 (1961).
[27] J. Rodriguez-Carvajal, Physica B **192**, 55 (1993).
[28] W. Dannhauser, and P. A. Vaughan, J. Am. Chem. Soc. **77**, 896 (1955).
[29] R. D. Shannon, Acta Crystallogr. Sect. A **32**, 751 (1976).
[30] H.-R. Oswald, P. Kuhn, and A. Reller, Solid State Ionics **32/33**, 528 (1989).
[31] J. M. R. Gonzalez, and C. O. Arean, J. Chem. Soc. Dalton Trans. **1985**, 2155 (1985).
[32] J.-P. Doumerc, A. Wichainchai, A. Ammar, M. Pouchard, and P. Hagenmuller, Mater. Res. Bull. **21**, 745 (1986).
[33] S. Mitsuda, H. Yoshizawa, N. Yaguchi, and M. Mekata, J. Phys. Soc. Jpn. **60**, 1885 (1991).
[34] S. Mitsuda, N. Kasahara, T. Uno, and M. Mase, J. Phys. Soc. Jpn. **67**, 4026 (1998).

[35]K. Kimura, H. Nakamura, K. Ohgushi, and T. Kimura, Phys. Rev. B **78**, 140401(R) (2008).

[36]M. Frontzek, G. Ehlers, A. Podlesnyak, H. Cao, M. Matsuda, O. Zaharko, N. Aliouane, S. Barilo, and S. V. Shiryaev, J. Phys.: Condens. Matter **24**, 016004 (2012).

[37]M. Poienar, V. Hardy, B. Kundys, K. Singh, A. Maignan, F. Damay, and C. Martin, J. Solid State Chem. **185**, 56 (2012).

[38]M. Poienar, F. Damay, C. Martin, J. Robert, and S. Petit, Phys. Rev. B **81**, 104411 (2010).

[39]M. Frontzek, J. T. Haraldsen, A. Podlesnyak, M. Matsuda, A. D. Christianson, R. S. Fishman, A. S. Sefat, Y. Qiu, J. R. D. Copley, S. Barilo, S. V. Shiryaev, and G. Ehlers, Phys. Rev. B **84**, 094448 (2011).

[40]R. S. Fishman, F. Ye, J. A. Fernandez-Baca, J. T. Haraldsen, and T. Kimura, Phys. Rev. B **78**, 140407(R) (2008).

[41]J. T. Haraldsen, F. Ye, R. S. Fishman, J. A. Fernandez-Baca, Y. Yamaguchi, K. Kimura, and T. Kimura, Phys. Rev. B **82**, 020404(R) (2010).